Earth and Planetary Science Letters 440 (2016) 33–42

Contents lists available at ScienceDirect

Earth and Planetary Science Letters

www.elsevier.com/locate/epsl

Surface uplift and convective rainfall along the southern Central Andes (Angastaco Basin, NW Argentina)

Heiko Pingel [a,*], Andreas Mulch [b,c], Ricardo N. Alonso [d], John Cottle [e], Scott A. Hynek [f], Jacob Poletti [e], Alexander Rohrmann [a], Axel K. Schmitt [g], Daniel F. Stockli [h], Manfred R. Strecker [a]

[a] Institut für Erd- & Umweltwissenschaften, Universität Potsdam, 14476 Potsdam, Germany
[b] Institut für Geowissenschaften, Goethe Universität Frankfurt, 60438 Frankfurt/Main, Germany
[c] Senckenberg Biodiversität & Klima Forschungszentrum (BiK-F), 60325 Frankfurt/Main, Germany
[d] Departmento de Geología, Universidad Nacional de Salta, 4400, Salta, Argentina
[e] Department of Earth Science and Earth Research Institute, University of California, Santa Barbara, CA 93106, USA
[f] Earth & Environmental Systems Institute and Department of Geosciences, Penn State University, University Park, PA 16802, USA
[g] Institut für Geowissenschaften, Universität Heidelberg, 69120 Heidelberg, Germany
[h] Department of Geological Sciences, University of Texas, Austin, TX 78712, USA

ARTICLE INFO

Article history:
Received 3 August 2015
Received in revised form 29 January 2016
Accepted 2 February 2016
Available online 15 February 2016
Editor: A. Yin

Keywords:
hydrogen stable isotopes
volcanic glass
paleoaltimetry
NW-Argentine Andes
orographic barrier uplift
convective rainfall

ABSTRACT

Stable-isotopic and sedimentary records from the orogenic Puna Plateau of NW Argentina and adjacent intermontane basins to the east furnish a unique late Cenozoic record of range uplift and ensuing paleoenvironmental change in the south-central Andes. Today, focused precipitation in this region occurs along the eastern, windward flanks of the Eastern Cordillera and Sierras Pampeanas ranges, while the orogen interior constitutes high-elevation regions with increasingly arid conditions in a westward direction. As in many mountain belts, such hydrologic and topographic gradients are commonly mirrored by a systematic relationship between the oxygen and hydrogen stable isotope ratios of meteoric water and elevation. The glass fraction of isotopically datable volcanic ash intercalated in sedimentary sequences constitutes an environmental proxy that retains a signal of the hydrogen-isotopic composition of ancient precipitation. This isotopic composition thus helps to elucidate the combined climatic and tectonic processes associated with topographic growth, which ultimately controls the spatial patterns of precipitation in mountain belts. However, between 25.5 and 27°S present-day river-based hydrogen-isotope lapse rates are very low, possibly due to deep-convective seasonal storms that dominate runoff. If not accounted for, the effects of such conditions on moisture availability in the past may lead to misinterpretations of proxy-records of rainfall. Here, we present hydrogen-isotope data of volcanic glass (δDg), extracted from 34 volcanic ash layers in different sedimentary basins of the Eastern Cordillera and the Sierras Pampeanas. Combined with previously published δDg records and our refined U–Pb and (U–Th)/He zircon geochronology on 17 tuff samples, we demonstrate hydrogen-isotope variations associated with paleoenvironmental change in the Angastaco Basin, which evolved from a contiguous foreland to a fault-bounded intermontane basin during the late Mio–Pliocene. We unravel the environmental impact of Mio–Pliocene topographic growth and associated orographic effects on long-term hydrogen-isotope records of rainfall in the south-central Andes, and potentially identify temporal variations in regional isotopic lapse rates that may also apply to other regions with similar topographic boundary conditions.

1. Introduction

The Andean Altiplano–Puna Plateau constitutes the most important orographic barrier in the southern hemisphere (e.g., Garreaud et al., 2010; Fig. 1A) and causes pronounced east–west rainfall and surface-process gradients (e.g., Bookhagen and Strecker, 2008, 2012). While the eastern plateau flanks are humid with rainfall of up to 3000 mm/yr in NW Argentina, the semi-arid to arid orogen interior transitions westward into one of the driest places on Earth, the Atacama Desert. Various plateau-evolution models have been proposed for the Andes (e.g., Isacks, 1988; Allmendinger et al., 1997), but the timing and style of uplift of the plateau and its flanking ranges remain controversial. For ex-

* Corresponding author.
E-mail address: heikop@geo.uni-potsdam.de (H. Pingel).

http://dx.doi.org/10.1016/j.epsl.2016.02.009
0012-821X/

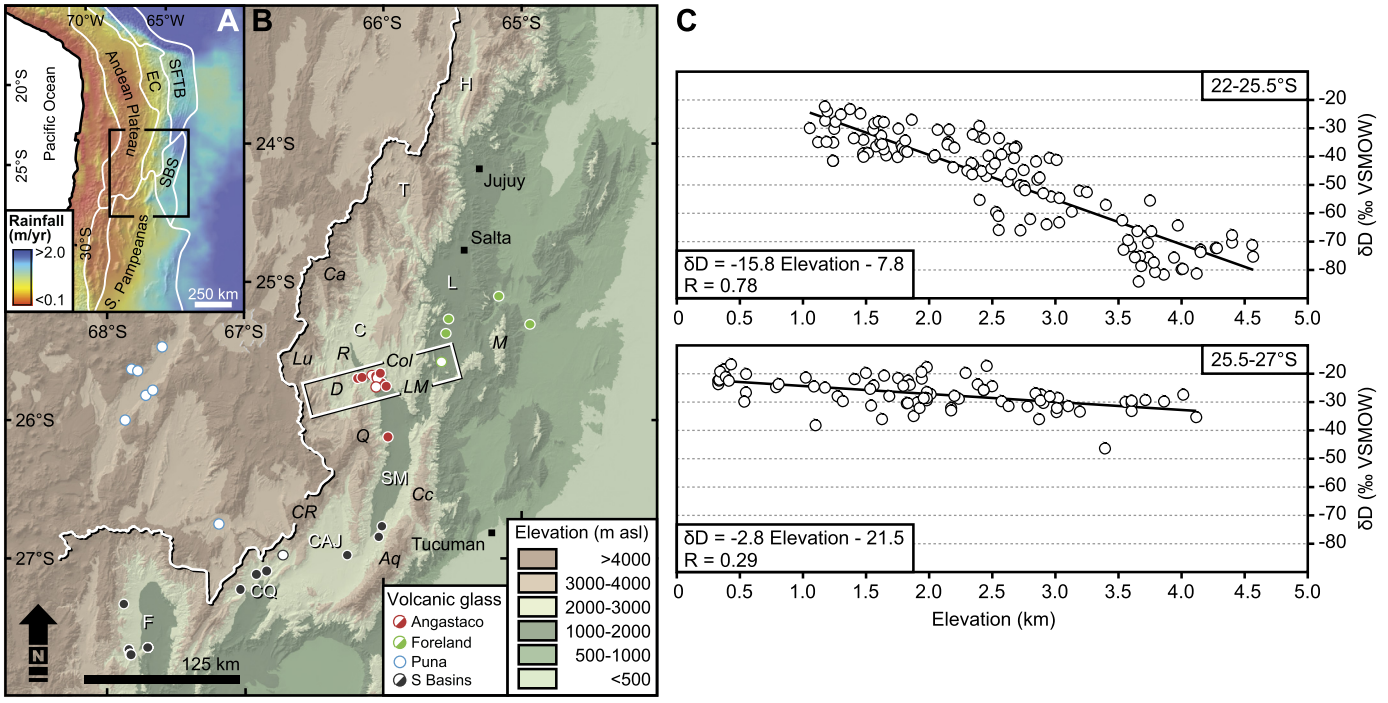

Fig. 1. (A) Morphotectonic map of southern Central Andes showing mean annual rainfall derived from NASA's (National Aeronautics and Space Administration) TRMM mission (Tropical Rainfall Measurement Mission) and extent of Fig. 1B (black box). EC—Eastern Cordillera, SFTB—Subandean fold-and-thrust belt; SBS—Santa Barbara System. (B) Digital elevation model with sample locations of isotopically dated Miocene to Pleistocene volcanic ash samples (filled: this study; open: Canavan et al., 2014; Carrapa et al., 2014) color-coded according to locations in the southern central Andes. White box indicates extent of Fig. 2. White letters denote sedimentary basins: H—Humahuaca; T—Toro; L—Lerma; C—Calchaquí (including the Angastaco Basin); SM—Santa María; CAJ—El Cajón; CQ—Corral Quemado; F—Fiambalá. Black letters indicate mountain ranges related to this study: Ca—Sierra de Cachi-Palermo; Lu—Cumbres de Luracatao; Col—Sierra de los Colorados; LM—Sierra León Muerto; R—Cerro Runno; D—Cerro Durazno; Q—Sierra Quilmes; Cc—Cumbres Calchaquíes; Aq—Sierra Aconquija; CR—Sierra Chango Real. (C) Hydrogen stable-isotope data from modern stream water between 22 and 27°S showing a strong latitudinal dependence of isotopic lapse rates across the eastern margin of the southern Central Andes (data from Rohrmann et al., 2014). (For interpretation of the references to color in this figure legend, the reader is referred to the web version of this article.)

ample, it is debated whether the southern sector of the plateau (Puna Plateau) has formed by crustal shortening during continuous lateral growth since Paleo–Eocene time (e.g., Reiners et al., 2015) or if this topographic growth had been accomplished by stepwise regional uplift associated with continental lithospheric delamination and the attainment of present-day elevations by ~36 Ma (Canavan et al., 2014; Quade et al., 2015). In either case, given the meridional orientation of the Andes and the principal trajectories of atmospheric circulation in the southern hemisphere, changes in topography must have fundamentally impacted biotic evolution and the climate and hydrologic systems on the windward and leeward sectors of the evolving orogen (e.g., Hoorn et al., 1995, 2010; Gregory-Wodzicki, 2000; Strecker et al., 2007; Baker et al., 2014).

In addition to classical stratigraphic and paleontological approaches with which to decipher plateau uplift, stable-isotope paleoaltimetry has become an indispensable method for the reconstruction of surface uplift of orogenic plateaus and their flanks (Chamberlain et al., 1999; Garzione et al., 2000; Gébelin et al., 2013; Hoke and Garzione, 2008; Mulch et al., 2008, 2004; Polissar et al., 2009; Quade et al., 2007; Rowley et al., 2001; Saylor and Horton, 2014; Cassel et al., 2014; Mulch, 2016). Typically, proxy-derived oxygen (δ^{18}O) or hydrogen (δD) isotope ratios are compared to present-day isotopic compositions of surface waters or modeled δ-values in precipitation assuming Rayleigh condensation and rainout of an adiabatically ascending air mass (e.g., Poage and Chamberlain, 2001; Rowley et al., 2001; Rowley and Garzione, 2007). However, among the many assumptions required to interpret paleoaltimetry results, a major problem in correctly assessing environmental change due to uplift is the complex interplay between surface uplift, atmospheric circulation, and orographic rainfall (Mulch, 2016). This combination of processes affects δ^{18}O and δD values of precipitation, and hence paleoelevation reconstructions. Moreover, many paleoaltimetry studies have focused on orogen interiors, while comparable analyses in the sedimentary fills adjacent to plateau-bounding ranges have been less common (e.g. Mulch et al., 2006; Hren et al., 2009). As a consequence, isotopic changes induced at orogenic margins (i.e., by topographic growth, atmospheric re-organization, and changes in isotopic lapse rates) may remain undetected in plateau environments or may not be interpreted as such.

Modern δ^{18}O and δD values in surface waters across the eastern Andean flanks between 22 and 28°S suggest that interactions between continental-scale atmospheric circulation and the topographic and thermal characteristics of areally extensive intermontane basins at the eastern plateau margin result in a gradual weakening of isotope-elevation relationships (lower isotopic lapse rates) with increasing latitude (Rohrmann et al., 2014; Fig. 1C). Accordingly, the modern river-based hydrogen isotope lapse rate between 25.5 and 27°S is very low (−2.8‰/km) compared to a pronounced rate north of 25.5°S (−15.8‰/km, Fig. 1C). This difference has been related to non-systematic effects of atmospheric convection characteristic of subtropical regions that interfere with orographic rainout along the eastern Andean flanks (Rohrmann et al., 2014). Evaluating past environmental conditions and paleoelevations under such conditions is challenging and requires understanding of how isotope lapse rates have changed over time.

Here, we present hydrogen stable isotope records from hydrated volcanic glass (δDg) extracted from intercalated volcanic ash-fall deposits in the Angastaco Basin (~25.7°S) in the Eastern Cordillera, the Lerma Basin in the adjacent broken Andean foreland (~25.5°S), and additional intermontane basins between

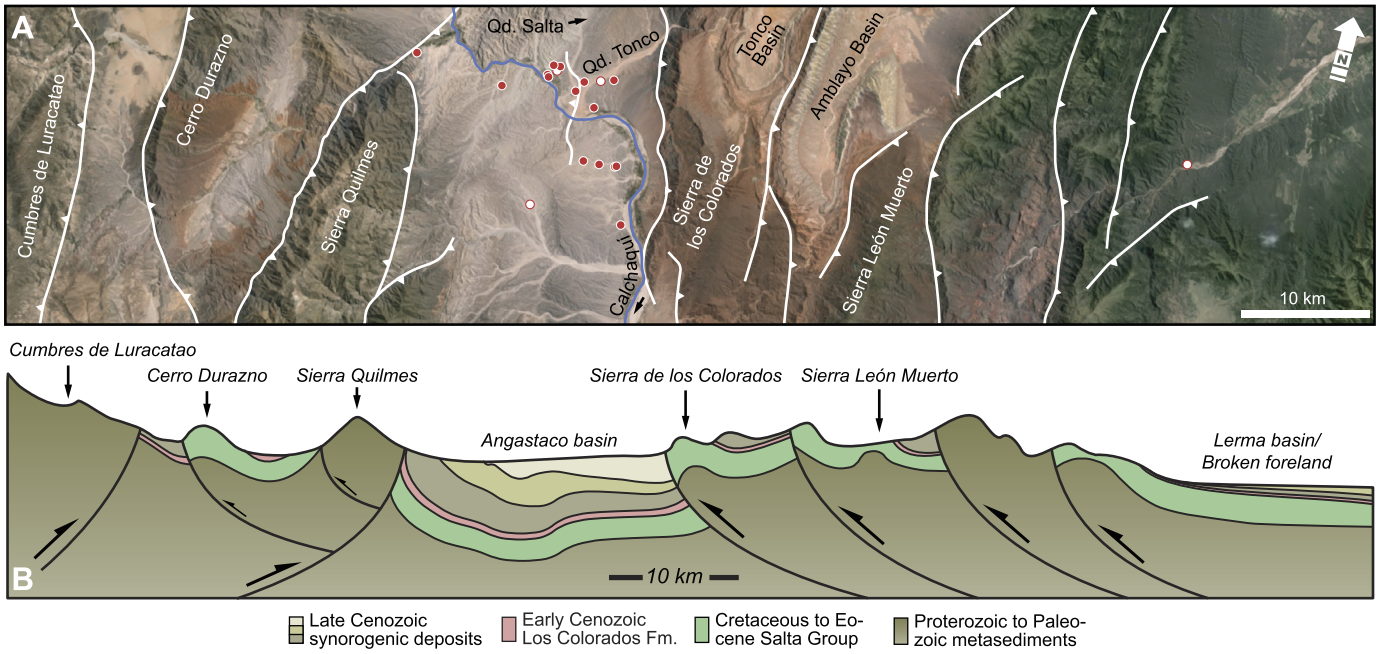

Fig. 2. (A) Satellite image of the Angastaco Basin and neighboring basins and ranges (Google Earth) showing range-bounding structures and locations of volcanic glass hydrogen stable-isotope samples from the Angastaco Basin used in this study. Circles in red denote samples from this study, white circles denote samples analyzed in Carrapa et al. (2014). (B) Schematic geological cross-section along Fig. 2A showing major basins and ranges (modified after Coutand et al., 2006; Deeken et al., 2006). (For interpretation of the references to color in this figure legend, the reader is referred to the web version of this article.)

25 and 28°S (Santa María, Cajón, Corral Quemado, and Fiambalá basins) that straddle the flanks of the southern Puna Plateau in NW Argentina (Fig. 1). During the Mio–Pliocene this region experienced pronounced deformation and basin compartmentalization, accompanied by the transition from a humid foreland to an elevated and hydrologically restricted, semi-arid intermontane basin (e.g., Bywater-Reyes et al., 2010; Carrapa et al., 2011; Coutand et al., 2006; Galli et al., 2011; Starck and Anzótegui, 2001; Strecker et al., 2007). Together with new U–Pb and U–Th/He zircon ages our data helps to constrain the patterns of topographic growth and associated change in moisture supply into the orogen along the eastern Andean flanks. In addition, a comparison of the Angastaco Basin record with coeval δDg results from the adjacent southern Puna Plateau (Canavan et al., 2014), reveals at least two episodes that resemble present-day stable isotope characteristics lacking signs of a pronounced isotope-elevation relationship. In keeping with the present-day conditions, we interpret these episodes in the context of enhanced convective rainfall.

2. Geologic background

The Angastaco Basin is an intermontane basin located in the Eastern Cordillera at 25.7°S at an elevation of ~1.8 to 2.0 km (Figs. 1 and 2). To the west, the Cumbres de Luracatao and other ~N–S-striking reverse fault-bounded mountain ranges (Quilmes, Durazno, and Runno) separate the Angastaco basin from the internally drained areas of the Puna Plateau. To the east, the basin is confined by the Sierra de los Colorados and Sierra León Muerto ranges that currently constitute an efficient orographic barrier at this latitude, causing enhanced rainout along their eastern, windward flanks and semi-arid conditions in the hinterland (e.g., Hain et al., 2011; Fig. 2). The basin contains a >7-km-thick sedimentary record (Fig. 3) documenting the protracted paleoenvironmental and structural history of late Cenozoic shortening at this latitude, whose onset is constrained by Eo–Oligocene deformation in the region that now constitutes the Puna margin (Coutand et al., 2006; Deeken et al., 2006; Hongn et al., 2007; del Papa et al., 2013). Sedimentation in the Angastaco area commenced during the late Eocene with redbeds of the Quebrada de los Colorados Formation in a largely contiguous foreland basin (Jordan and Alonso, 1987; Deeken et al., 2006; del Papa et al., 2013). Deformation along the present-day Puna margin (Cumbres de Luracatao) resulted in structural separation of the Puna from the foreland after ca. 20 Ma (Coutand et al., 2006; Deeken et al., 2006; Galli et al., 2014). By ~14 to 13 Ma fluvial sandstones and conglomerates of the Angastaco Formation, mainly sourced from the uplifting Cumbres de Luracatao to the west, were unconformably deposited onto older sedimentary units (Fig. 3; Coutand et al., 2006; Deeken et al., 2006; Galli et al., 2014). This unconformity is also recorded in the uplifted Amblayo and Tonco basins east of Angastaco (Fig. 2), implying at least mid-Miocene deformation and erosion in the area of the Sierra de los Colorados and Sierra León Muerto ranges (Galli et al., 2014). Additionally, clast provenance in the Tonco area locally records westward paleocurrent directions in the Angastaco Formation by ~10 Ma (Galli et al., 2014). This supports the notion of existing local topography at 10 Ma, which is also confirmed by rapid exhumation of the Sierra de los Colorados since ca. 12–10 Ma and the Sierra León Muerto since ca. 8–6 Ma (Carrapa et al., 2011). To the west, apatite fission-track data record exhumation of the Quilmes, Durazno, and Runno ranges beginning between 12 and 7 Ma, which is corroborated by clast provenance and detrital apatite fission-track thermochronology in the Angastaco Formation (Coutand et al., 2006; Deeken et al., 2006).

The Angastaco Formation is overlain by fluvial mudstones and sandstones of the Palo Pintado Formation (Fig. 3, ca. 9–5.2 Ma, Coutand et al., 2006). Sedimentological evidence and the fossil record suggest that parts of this unit were deposited under humid conditions, characterized by north to northeast-directed drainages (Fig. 3), low-energy river systems, swamps, and lakes (e.g., Carrapa et al., 2012; Galli et al., 2014; Starck and Anzótegui, 2001). Deposition of the overlying San Felipe Formation, since ca. 5.2 Ma (Fig. 3; Bywater-Reyes et al., 2010), followed an episode of basin-internal deformation, as documented by a regional angular un-

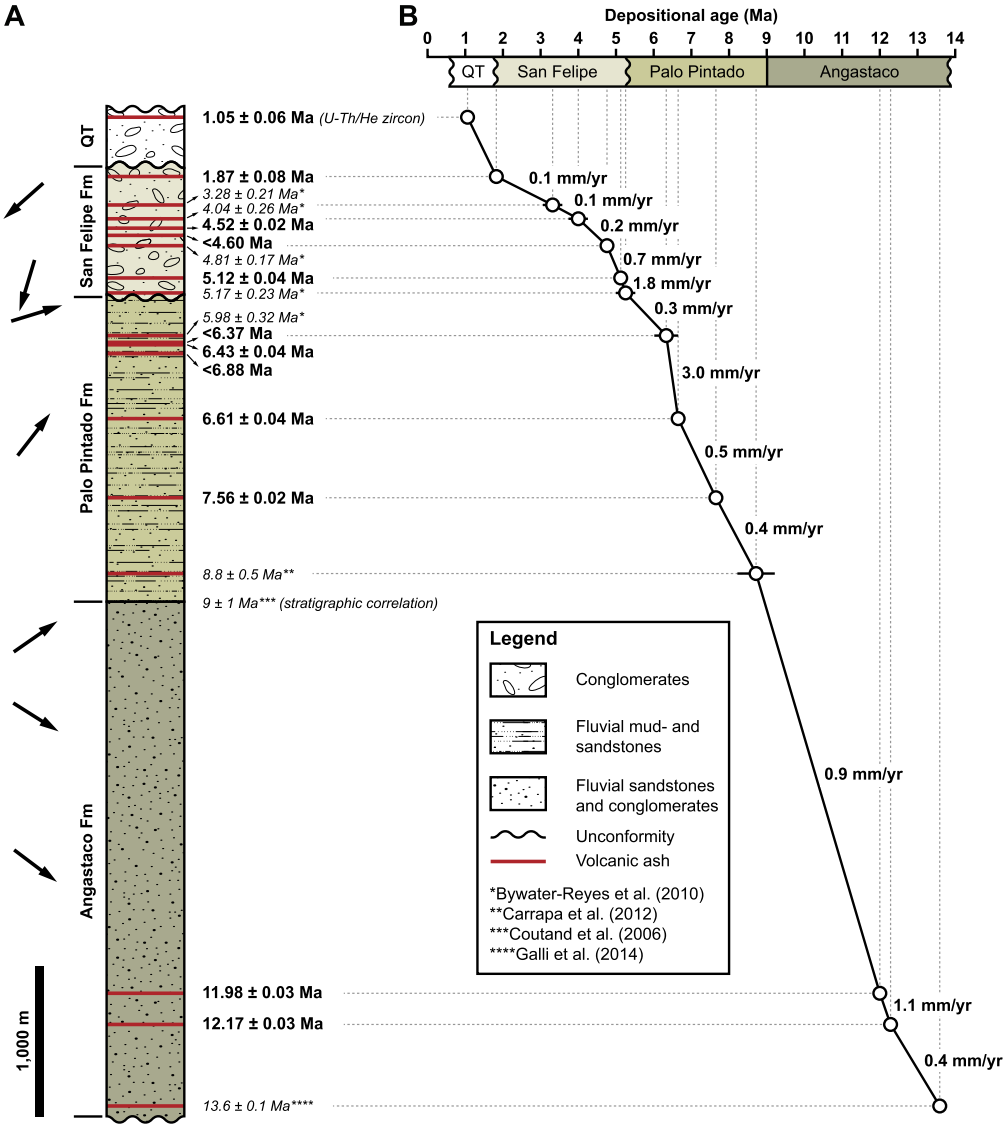

Fig. 3. (A) Generalized stratigraphy of the Angastaco Basin showing radiometric depositional age estimates of volcanic ash deposits presented in this study (bold) and from previous studies (italics, Coutand et al., 2006; Bywater-Reyes et al., 2010; Carrapa et al., 2012; Galli et al., 2014). If not otherwise indicated, all ages are derived from U–Pb zircon geochronology. Arrows represent average paleocurrent directions from Carrapa et al. (2012), highlighting the change towards axial, southward drainage after about 5.2 Ma. (B) Geochronology vs. stratigraphic thickness plot showing sediment-accumulation rates (mm/yr). Error bars represent 2σ error. QT—Quaternary terrace conglomerates.

conformity (Carrera and Muñoz, 2008). At about the same time (~5 Ma) Puna-sourced metamorphic and volcanic clasts disappear from the sedimentary record of the neighboring Lerma Basin to the east (Fig. 1; Hain et al., 2011). These observations document the separation of the two regions by a contiguous topographic barrier east of the Angastaco Basin (Sierra de los Colorados and Sierra León Muerto ranges). This interpretation is supported by the appearance of clasts from the Cretaceous Salta Group within sections of the San Felipe Formation in the Quebrada de Salta (Fig. 2), near the present-day eastern Angastaco-basin margin that are associated with west- to southwest-oriented sediment transport from source regions within the Sierra de los Colorados and Sierra León Muerto ranges (Fig. 3; Carrapa et al., 2012; Galli et al., 2014). By ca. 4 Ma the conglomerates of the San Felipe Formation record a more widespread appearance of easterly-derived clasts (Bywater-Reyes et al., 2010). Moreover, sedimentological evidence suggests the onset of arid conditions associated with orographic effects along the eastern basin-bounding ranges (Coutand et al., 2006; Starck and Anzótegui, 2001). Further shortening in the Eastern Cordillera resulted in basin-internal deformation and erosion marked by a regional unconformity with overlying Quaternary conglomerates (reviewed in Coutand et al., 2006). Subsequently, these gravels were partially eroded and removed from the basin, documenting renewed fluvial connectivity with the foreland that characterizes the Angastaco Basin today.

3. Climatic conditions

Easterly winds, associated with the South American Monsoon, transport moisture from the Atlantic Ocean across the Amazon Basin towards the eastern flanks of the Andes, where orography causes a southward deflection to form the South American low-level jet (Fig. 4A; Vera et al., 2006). During austral summer (Dec–Feb) this jet follows the eastern Andean flanks and transports moisture into subtropical South America (e.g., Vera et al., 2006), accounting for >80% of the annual rainfall in this region (Prohaska, 1976). Westward transport of these air masses across the Andes re-

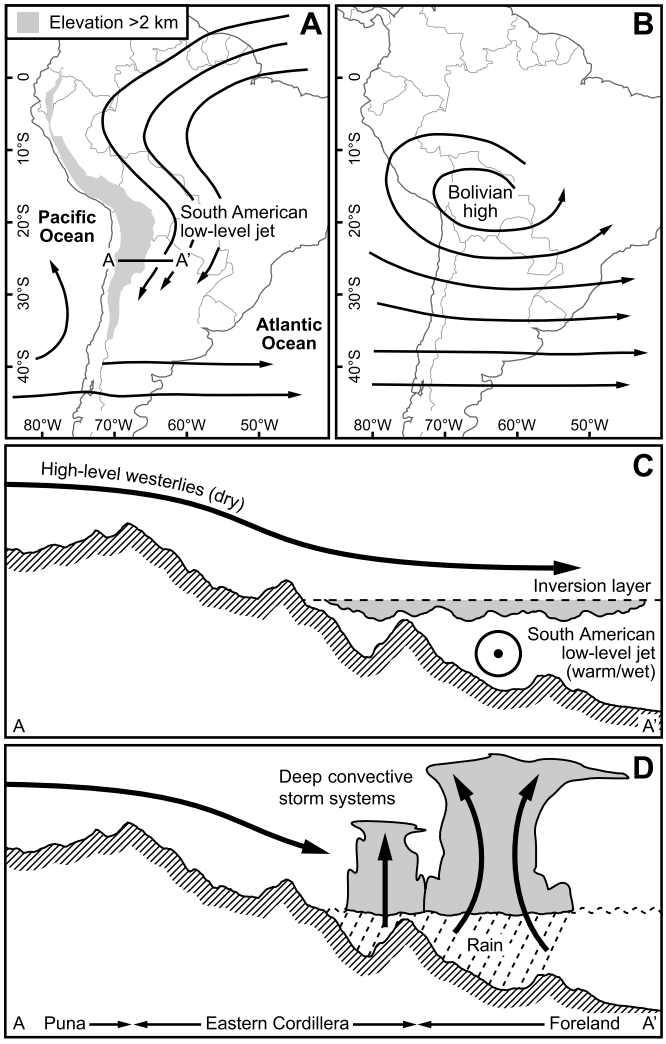

Fig. 4. (A), (B) Generalized patterns of South American atmospheric circulation during austral summer (Dec–Feb). (A) Low-level winds at 850 hPa and (B) high-level winds at 200 hPa (modified after Fiorella et al., 2015). (C), (D) Conceptual model of deep-convective rainfall south of ca. 25.5°S, where the descent of dry and cold westerly winds (C) prevents moisture-bearing, warm air masses of the Andean low-level jet to rise, until (D) sufficient thermal energy (from solar heating) causes strong vertical upward motion of moisture and the formation of deep-convective storm systems (modified after Rohrmann et al., 2014).

sults in enhanced orographic rainout along the eastern flanks and progressively arid conditions towards the orogen interior (Fig. 1A; Bookhagen and Strecker, 2008). In NW Argentina this gradient is expressed by annual rainfall of more than 1300 mm/yr along the eastern flanks of the Eastern Cordillera and Sierras Pampeanas, and less than 200 mm/yr in the orogen interior (Fig. 1A).

In addition, the subtropical regions east of the Andes are affected by high-level westerly winds that transport dry air across the orogen (Fig. 4B; Romatschke and Houze, 2010). Downslope airflow across the eastern flanks causes an atmospheric inversion that prevents humid air of the South American low-level jet from ascending (Fig. 4C), until it is rapidly lifted (Fig. 4D), e.g. by solar heating (Rohrmann et al., 2014). This energy release results in extreme hydro-meteorological events (deep convective storms), which presently appear to be the cause for most of the annual rainfall in the subtropical eastern Andes south of ca. 25.5°S (Fig. 4C; Rohrmann et al., 2014; Romatschke and Houze, 2013). At present, neither the onset of the convective conditions is known, nor is there robust evidence for a manifestation of this phenomenon on longer timescales.

4. Stable isotopes in hydrated volcanic glass

Stable isotope paleoaltimetry is derived from a commonly observed negative relationship between $\delta^{18}O$ and δD values in precipitation or surface waters (δDw) and elevation, which results from progressive condensation (Rayleigh distillation) and rainout of an ascending air mass (e.g. Rowley et al., 2001; Poage and Chamberlain, 2001; Rowley and Garzione, 2007). Following eruption and subsequent deposition, volcanic glass from silicic ash-fall deposits incorporates large amounts of water by diffusion (up to 10 wt%) and becomes saturated over ~1–10 kyr, after which insignificant hydrogen exchange occurs with younger surface water (e.g. Friedman et al., 1993). Moreover, it has been shown that hydrogen undergoes systematic isotope fractionation during the glass-hydration process, described by the empirically determined fractionation equation of Friedman et al. (1993), $\delta Dw = 1.034\ (1000 + \delta Dg) - 1000$, whereby δDg represents a time-integrated signal of δDw values of ancient meteoric water (e.g. Friedman et al., 1993; Mulch et al., 2008; Dettinger and Quade, 2015). Finally, δDg values appear to be resistant to diagenetic alteration and are preserved over geological timescales (e.g., Friedman et al., 1993; Mulch et al., 2008) in semi-arid environments, which makes volcanic glass an ideal proxy material for the reconstruction of paleoenvironmental conditions and the examination of feedbacks between tectonic processes and climate (Cassel et al., 2009, 2014; Friedman et al., 1993; Mulch et al., 2008; Pingel et al., 2014).

5. Analytical methods

5.1. Geochronology of volcanic ash deposits

To refine the chronology of the investigated stratigraphic sections, we use U–Pb and (U–Th)/He dating on zircons from volcanic ash samples. Zircon grains were handpicked, mounted in epoxy, and polished for U, Th, and Pb isotope analysis using a Laser Ablation Multi-Collector Inductively Coupled Plasma Mass Spectrometer (LA-MC-ICPMS), during two analytical sessions, at the University of California, Santa Barbara. Moreover, about 30 crystals per sample were handpicked, mounted in epoxy, polished and cleaned, and then gold-coated for ion-microprobe analysis. Crystals free of inclusions or cracks were selected for U–Pb analysis, using the CAMECA IMS 1270 ion microprobe at the University of California in Los Angeles (U–Pb SIMS). Due to significant pre-eruptive residence times and/or post-eruptive reworking most analyzed samples show a complex pattern of U–Pb zircon age distributions. Therefore, we systematically excluded the oldest ages from our calculations of an average zircon crystallization age until near-unity values for the mean square of weighted deviates (MSWD < 2) were achieved. In cases, where no coherent young population was found, we selected the youngest $^{206}Pb/^{238}U$ zircon ages to represent a maximum depositional age. Finally, Zircon (U–Th)/He (ZHe) analysis of a single sample was performed at the Isotope Geochemistry Laboratory of the University of Kansas. All analytical results and further methodological information can be found in the supplementary material.

5.2. Hydrogen isotope analysis of volcanic glass shards

Volcanic ash samples were crushed, sieved, and treated with 10% hydrochloric acid for 15 min and 5% hydrofluoric (HF) acid for 30 s in an ultrasonic bath to remove altered rims and adherent carbonate and clay minerals. Subsequently, samples were rinsed with deionized water and dried. For separates that needed further concentration, standard magnetic and density techniques were applied. Glass shards (125–250 µm) were handpicked using a cross-polarizing microscope. About 1.5 mg of each sample was packed

in silver cups, loaded, and released to a helium-purged Thermo-Finnigan TC/EA (high-temperature conversion/elemental analyzer) equipped with a Costech zero-blank auto sampler. The extracted sample gas was admitted into a Thermo-Finnigan ConFlo III connected in continuous-flow mode to a Thermo-Finnigan MAT 253 stable-isotope mass spectrometer. Five internationally referenced standard materials and laboratory working standards were run with our samples, random samples were duplicated and tested for consistency, and the raw isotope data were corrected for mass bias, daily drift of the thermal combustion reactor, and offset from the certified reference values. After correction, NBS30 (biotite), CH-7 (polyethylene), and NBS22 (oil) reference materials yielded $\delta D = -64.3 \pm 0.8‰$, $-104.5 \pm 0.6‰$, and $-117.5 \pm 1.1‰$, respectively. Repeated measurements of standards yielded a precision of $\pm 3.0‰$ for δDg. With one exception, duplicates of selected unknowns (2–3 duplicates/sample) were reproduced at precisions of $<3.0‰$. Finally, we calculated differential δDg values ($\Delta\delta D_{A\text{-}P}$) of the Angastaco and early foreland δDg data (when both regions belonged to a contiguous foreland basin) with coeval records from the high-elevation southern Puna Plateau (Canavan et al., 2014), which helps to evaluate temporal changes in isotope lapse rates (Mulch, 2016). All isotope measurements were performed at the Joint Goethe University-BiK-F Stable Isotope Facility, Frankfurt. All isotopic ratios are reported relative to V-SMOW (Supplementary Table 1).

6. Results

6.1. Geochronology

We present 13 new U–Pb zircon ages and one ZHe age from the Angastaco Basin that refine the stratigraphy in this region (Fig. 3). Two samples from the lower Angastaco Formation, 12.17 ± 0.03 Ma (Ang-080313-1) and 11.98 ± 0.03 Ma (Ang-Isa-7-R), are consistent with previous age estimates for this section based on sedimentation rates (Coutand et al., 2006). Five new ages refine the age of the Palo Pintado Formation with estimates ranging between ca. 7.6 and 6.4 Ma (Ang-080313-3, Ang-080313-2, Ang-070313-4, Ang-070313-2, Ang-070313-3). Four tuff samples from the San Felipe Formation yield U–Pb ages between ca. 5.1 and 1.9 Ma (Ar-11-Ash-2/3, Ar-11-Ash-4, Ar-11-Ash-5, Ang-070313-1), refining the upper limit of this unit. Sample 005 (ZHe $= 1.05 \pm 0.06$ Ma) is from a Quaternary fill unit along the western basin margin that unconformably overlies a deformed section of the lower Angastaco Formation near the thrust front of the northern sector of the Quilmes range. Sample Vc-050313-1 is from a white, unconsolidated ash layer interbedded in a young alluvial-fan deposit at the eastern foothills of the Quilmes range. Our results for this sample imply a depositional age below the limit of the LA-ICPMS method for our setup (<0.7 Ma). Hence, the age range for the sample is 0.35 ± 0.35 Ma, which is consistent with its geomorphic position in the landscape.

We also obtained a new U–Pb age estimate from a deformed section of the Guanaco Formation at the eastern foothills of the Metán Range in the broken foreland (Figs. 1 and S1). The three youngest zircons of this sample (Ar-14-Ash-1) yield an age of 7.39 ± 0.03 Ma, which contrasts the formerly proposed 8.73 ± 0.25 Ma for this ash (Viramonte et al., 1994). Moreover, we present two U–Pb SIMS ages from the Corral Quemado area (Fig. 1). Sample CQ12 was collected ca. 10 km west of the village of Puerta Corral Quemado in the late Miocene Chiquimil Formation; its two youngest zircons suggest a maximum age of 8.74 ± 0.53 Ma. Sample CQ38 was collected about 12 km north of Puerta Corral Quemado in the Corral Quemado Formation and yields an age of 3.65 ± 0.12 Ma. For a stratigraphic overview of the age estimates in our study please refer to Figs. 3 and S1. Additional details on the stratigraphic context of the samples can be found in the supplementary material.

6.2. δD of volcanic glass

We measured δDg values of 17 volcanic glass samples from ash beds in late Miocene to Pleistocene sediments from the Angastaco Basin, currently at elevations between 1.7 and 1.9 km. Combined with recently published data from this basin (Carrapa et al., 2014), this enables us to evaluate a well-dated δDg record of 24 glass samples from the Angastaco Basin covering the last $\sim 8.8 \pm 0.5$ Myr (red, Fig. 5). This record shows that relatively stable isotopic conditions ($\delta Dg = -75 \pm 3‰$) until 6.5 Ma were followed by periodic δDg shifts ranging between $-95‰$ and $-65‰$.

Four samples from present-day foreland regions east of the Angastaco Basin, at elevations between 0.75 and 1.25 km, show a narrow range of δDg values between -78 and $-75‰$ over the last 9.3 Myr (green, Fig. 5). Data from Carrapa et al. (2014) reveal a similar value in the present-day foreland region at 14.4 ± 0.6 Ma ($\delta Dg = -78‰$).

In addition, we determined δDg values of 13 glass samples from other intermontane basins adjacent to the southern Puna Plateau (grey, Fig. 5) in the Santa María ($n = 3$), El Cajón ($n = 1$), Corral Quemado ($n = 4$), and Fiambalá basins ($n = 5$). Including data from the Corral Quemado area (Carrapa et al., 2014), we are able to present a dataset from $\sim$8.5 to 3.5 Ma with a δDg range of -95 to $-70‰$. Note that major δDg trends in the southern basins are very similar to the Angastaco δDg record (Fig. 5A).

A potential concern for such comparisons may originate from the analysis of absolute δDg values of different studies and laboratories. Whether the use of hydrofluoric acid (HF), as a pretreatment step to purify volcanic glass fractions of altered rinds and adherent secondary minerals is a necessity to approach 'true' δDg values or the cause of additional problems is matter of an ongoing debate. While one view holds that HF treatment is a prerequisite of obtaining reliable δDg values as untreated samples may be biased by isotopically-open hydration rinds and δDg values may be shifted towards present-day δD precipitation values (e.g., Cassel et al., 2014), Dettinger and Quade (2015) suspect HF treatment to be a potential source for increased scatter in δDg data. Although our study was not designed to investigate this problem, we have reason to believe that a comparison of our data with non-HF derived isotope values from Carrapa et al. (2014) and Canavan et al. (2014) may be justified. Four of our samples are resampled volcanic ashes (AT3-9-R, AT2-7-R, AT4-3-R, and AT7-10-R) previously collected by Carrapa et al. (2014). New δDg values are indistinguishable from the equivalent samples (AT3-9, AT2-7, AT4-3, and AT7-10) presented in Carrapa et al. (2014). Only one sample pair (AT4-3-R and AT4-3) shows a larger difference in δDg of 11.5‰. However, the 1σ-error of AT4–3 ($-76.5 \pm 8.0‰$) exceeds 10%, suggesting contamination. Deviations of the three other pairs are $<3.0‰$, which lead us to conclude that in the present case a comparison between the two sample sets provides meaningful results.

7. Discussion

7.1. Hydrogen stable isotope record

Because hydrogen stable isotope ratios of volcanic glass are closely linked with the isotopic composition of meteoric water present during hydration, temporal changes in δDg can often be associated with the interplay between regional tectonics and surface uplift (e.g., Cassel et al., 2009, 2014; Mulch et al., 2008; Pingel et al., 2014). In addition, climatic factors such as changes in global/regional air and sea-surface temperatures, and changes in the location of the water-vapor source or air-parcel trajectories

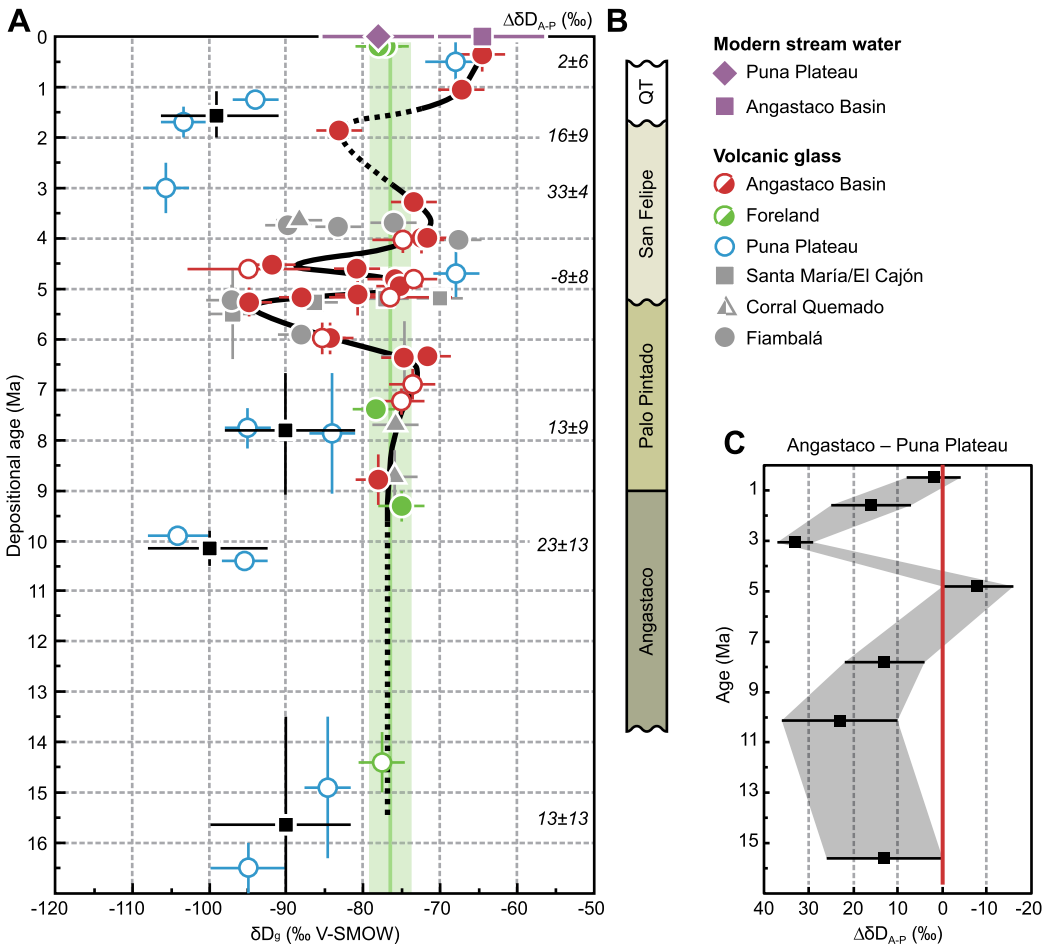

Fig. 5. (A) Hydrogen stable isotope compositions of volcanic glass (δDg) color-coded for sampling locations. Filled symbols are from this study and open symbols from Canavan et al. (2014) and Carrapa et al. (2014). Black curve shows interpretation of main trends in the Angastaco data with high δDg variability since ca. 6.5 Ma. Green line and shaded area depict mean δDg and $\pm$2sd of samples from the present-day foreland (green). Black squares and error bars represent binned averages of enclosing Puna samples (blue). To calculate the δDg difference between the Angastaco and Puna record ($\Delta\delta D_{A\text{-}P}$), δDg of binned averages and remaining individual data points were subtracted from adjacent Angastaco δDg values. (B) Schematic illustration of the Angastaco Basin record to compare major depositional events in the basin with the δDg record. Formation boundaries are plotted according to their stratigraphic age as shown in Fig. 3B. Note that the positive shift at ~5 Ma coincides with the onset of conglomerate deposition of the San Felipe Formation under semi-arid conditions. (C) $\Delta\delta D_{A\text{-}P}$ vs. age plot identifies similar δD values in precipitation at ca. 5 Ma and during the Quaternary in the Angastaco and Puna regions, implying low isotope lapse rates. (For interpretation of the references to color in this figure, the reader is referred to the web version of this article.)

across the Amazon Basin will inevitably influence hydrogen-isotope ratios of meteoric water across the eastern Andean margin. To a first order, such source-related changes are likely to result in regionally significant and synchronous δD shifts in precipitation. These are, however, not observed in late Miocene to Pleistocene stable isotope records in NW Argentina. On the contrary, between ca. 6 and 3 Ma, the δDg record from the intermontane Humahuaca Basin, ca. 250 km northeast of the Angastaco Basin, attains δDg values that are characterized by a general trend of deuterium depletion without signs of significant variability as seen in the Angastaco record (Pingel et al., 2014).

More evidence is furnished by the sedimentary record of intermontane basins and foreland sectors along the southern central Andes, which suggests that the low-level jet was established between 10 and 8 Ma, implying that the eastern Andes had gained sufficient elevation at that time (Mulch et al., 2010; Starck and Anzótegui, 2001; Uba et al., 2007; Bona et al., 2013). It is therefore unlikely that moisture source and transport directions for this sector of the orogen have changed fundamentally since the late Miocene. Moreover, there is no evidence for shifts of sufficient magnitude in the marine oxygen-isotope record during the considered time interval (e.g., Zachos et al., 2008). For these reasons, we interpret the results of our analysis in the context of surface uplift and ensuing climate change.

One complication in interpreting stable isotopes in precipitation records from this region concerns spatially variable modern isotope lapse rates, especially south of 25.5°S, where deep convection processes appear to represent the main mode of present precipitation (Rohrmann et al., 2014; Fig. 4). To investigate the temporal variability of this phenomenon at this latitude, we compare δDg values from the intermontane basins and the adjacent low-elevation foreland with coeval data from the high-elevation Puna Plateau (Canavan et al., 2014). The calculated $\Delta\delta D_{A\text{-}P}$ values vary considerably over time and range between -8‰ and $+33$‰ (Fig. 5). Our results show that low $\Delta\delta D_{A\text{-}P}$ values correlate well with δDg maxima in both regions, and indicate at least two episodes with reduced isotopic lapse rates that are characteristic of present-day conditions. These occurred at about 5.0 ± 0.5 Ma and during the changeover to the present-day conditions at approximately 1 Ma. Both time intervals are characterized by equally high δDg values (-70 ± 5‰) in the Angastaco Basin and the Puna Plateau, with low differential δDg values ($\Delta\delta D_{A\text{-}P}$) of $+2$‰ and -8‰ (Fig. 5). In contrast, other episodes generally exhibit more negative values on the plateau compared to the intermontane basin record with $\Delta\delta D_{A\text{-}P}$ of ca. $+20$‰, which reflects the general elevation

difference between these regions. This suggests that the present-day low isotope lapse rates may represent a recurring, rather than a sustained phenomenon that results from convection-dominated rainfall.

From north to south, the Santa María (26.5°S), El Cajón, Corral Quemado (27°S), and Fiambalá basins (27.5°S) constitute a group of intermontane basins in the Sierras Pampeanas, adjacent to the southern Puna Plateau (Fig. 1). Although, the δDg records from these basins are insufficient to discuss their individual basin development associated with the uplift of orographic barriers, an important observation can be made when comparing the data with the Angastaco record. First, the records from these basins complement each other (grey, Fig. 5). For example, between ~8.5 and 6.5 Ma, δDg values remain consistently at $-75‰$ and subsequently decrease until ca. 5.3 Ma, followed by a rapid positive shift in δDg. This suggests that processes impacting δDg values in the Angastaco Basin may also have been active in similar morphotectonic settings farther south. Second, these findings are corroborated by similar trends in the stable isotope records of tooth enamel and soil carbonates, from the Corral Quemado area and the Santa María Basin, respectively (Hynek, 2011; Hynek et al., 2012). These data document transient episodes of oxygen and carbon heavy-isotope enrichment between 5.6 and 5.2 Ma and possibly at about 4 Ma that are consistent with phases of deuterium enrichment observed in the glass record from the Angastaco Basin.

7.2. Surface uplift, basin aridification and enhanced convection

Previous work on δDg in the Angastaco area suggested similar-to-modern elevations (~2 km a.s.l.) since 14–10 Ma (Carrapa et al., 2014). In contrast, our improved δDg record provides evidence for major paleoenvironmental change, which includes surface uplift, enhanced aridity associated with windward orographic barrier uplift to the east, and conditions favoring convective rainfall in this region.

Mid-Miocene to Pleistocene glass samples from the present-day broken foreland (Fig. 1) show little isotopic variation (mean $\delta Dg = -77 \pm 3‰$ [2sd], Fig. 5) and are within error of calculated modern δDg estimates of $-67 \pm 11‰$ (based on modern stream-water data, Rohrmann et al., 2014). This, and the fact that the current foreland of NW Argentina has undergone only minor surface uplift compared to the orogen interior (Hain et al., 2011; Strecker et al., 2009), supports our inference that the environmental forcing factors in this region remained largely constant over the course of the last ~14.4 Myr. Moreover, our combined Angastaco and foreland basin δDg record shows no major trends (mean δDg of $-76 \pm 2‰$) until ~6.5 Ma. This supports the notion that surface elevations in the Angastaco area did not significantly depart from the rest of the former foreland, which is consistent with the circumstance that the Angastaco Formation (13–9 Ma) was deposited in a largely contiguous foreland basin.

Between ~6.5 and 5.3 Ma, δDg values from the Angastaco Basin decrease by $-23 \pm 6‰$ (absolute $\delta Dg = -95‰$), which we interpret to be the result of surface uplift in this area. First, the deviation of δDg values in the Angastaco record from that of the foreland samples imply a local cause that rules out the potential impact of global climate change or changes in the source-water region and/or its isotopic composition. Secondly, the timing of deuterium depletion in the Angastaco Basin is consistent with the late Miocene onset of deformation of basin-bounding ranges as suggested by low-temperature thermochronology. For example, rapid exhumation of the Cerro Durazno and Sierra de Quilmes ranges to the west commenced between 12 and 7 Ma (e.g., Coutand et al., 2006; Deeken et al., 2006). Deformation along the present-day eastern basin margin caused rapid exhumation beginning at ca. 12 Ma (Carrapa et al., 2011). The lag time between onset of exhumation and the establishment of significant topography, could have been caused by prior removal of the sedimentary cover, before more resistant bedrock was exposed (Deeken et al., 2006). Protracted shortening affected inherited structures underneath the Angastaco Basin prior to 5–6 Ma, which led to basin-internal deformation (e.g., Carrera and Muñoz, 2008). Finally, an increase in sediment-accumulation rates from 0.5 to 3.0 mm/yr at ca. 6.6 Ma might indicate growing accommodation space as a result of tectonic basin fragmentation at that time (Fig. 3B).

After ca. 5.3 Ma our δDg record is characterized by a rapid shift of $+22 \pm 6‰$ from -95 to $-73‰$ at ~4.8 Ma. Previous studies related such shifts to enhanced aridification caused by the establishment of threshold elevations on the windward side and associated orographic shielding (Pingel et al., 2014). In the Angastaco Basin this positive δDg shift is coeval with the onset of coarse gravel and conglomerate deposition of the San Felipe Formation (Bywater-Reyes et al., 2010; Coutand et al., 2006). Moreover, we found a ca. 30-cm-thick halite-bearing layer in a dated section of the San Felipe Formation (4.8 ± 0.2 Ma U–Pb zircon, Bywater-Reyes et al., 2010) at 25.7294°S, 66.0191°W, which supports this notion. Therefore, a paleo-environmental scenario is reasonable during which tectonically-induced aridity caused deuterium enrichment in the Angastaco Basin record through enhanced soil–water or sub-cloud evaporation (e.g., Quade et al., 2007; Schemmel et al., 2013). This inference is further supported by soil carbonate stable isotope results from the Angastaco Basin that suggest sustained aridity by ca. 5 Ma (Bywater-Reyes et al., 2010). In such a setting, it is reasonable to infer that the subsequent variability in the Angastaco δDg record (Fig. 5) was caused by changes in moisture supply into the basin, associated with shifts in the amount of evaporation of surface water.

Alternatively, at about 4.7 ± 0.5 Ma unusually high δDg values are recorded for deposits on the Puna Plateau ($-68‰$; Canavan et al., 2014) that overlap with our intermontane basin record. At this time the Puna Plateau had already gained most of its present-day elevation (Montero-López et al., 2014), therefore, this isotopic configuration would be consistent with non-systematic hydrogen-isotope fractionation with elevation, which is intriguingly similar to present-day conditions in this region. Thus, in light of the present-day convective setting, we propose paleo-environmental conditions that facilitated enhanced convective rainfall that forced positive shifts in the Angastaco δDg record.

7.3. Quantitative paleoaltimetry constraints

Complexities in the δDg record, caused by atmospheric patterns and enhanced aridity in the lee of growing topography, prevent us from estimating paleoelevations between 25 and 28°S by assuming purely adiabatic processes for the entire δDg record. Consequently, it is challenging to quantify elevation change between the low-elevation foreland and the elevated Angastaco Basin. However, the fact that neither the strong variability nor unusually low lapse rates are observed prior to 6.5 Ma is compatible with the proposition that convective rainfall in NW Argentina is largely caused by the interaction of atmospheric air-flow patterns and solar heating of intermontane basins along the flanks of the Puna Plateau (Rohrmann et al., 2014). This suggests that (a) fully developed semi-arid basins prone to solar heating and located at transitional elevations between the foreland and the plateau region did not exist until 5 Ma (e.g., Strecker et al., 2009) and/or (b) that the atmospheric conditions did not favor convective rainfall.

Minimal non-systematic isotope effects in precipitation (i.e., convective rainfall) may be inferred for the interval between 6.5 and 5.3 Ma when the Angastaco Basin records a strong negative shift in δDg during the transition to an intermontane-basin setting.

Using the modern hydrogen lapse rate (−15.8‰/km) determined for the region between 22 and 25.5°S (Fig. 1C, Rohrmann et al., 2014) we estimate the relative elevation change between the low-elevation, broken-foreland sector, and the intermontane Angastaco Basin at that time to be on the order of 1.5 ± 0.4 km. Despite the large uncertainties associated with this approach, our estimate is within the possible range of the expected surface uplift from a former, low-elevation foreland at ca. 0.5 to 1.0 km and the current elevation of the Angastaco Basin at 1.8 to 2.0 km.

8. Conclusions

The δDg record from intermontane sedimentary basins adjacent to the southern Puna Plateau in NW Argentina reveals a complex relationship between the hydrogen stable-isotope composition of volcanic glass (δDg), tectono-sedimentary events, orographically induced climate change, and the effects of enhanced convective rainfall. Collectively, this renders meaningful interpretations of δDg from these intermontane basins alone challenging, despite the ubiquitous availability of environmental proxy indicators. The parallel trends of positive δDg shifts observed on the plateau and the adjacent lower-elevation basins indicate at least two episodes that suggest enhanced convective processes at about 5 Ma and, consistent with present-day conditions, beginning at 1 Ma. Excluding these time intervals from our paleoaltimetric interpretations, we suggest similar initial elevations of the present-day foreland and the intermontane Angastaco Basin until ca. 6.5 Ma. This was followed by km-scale surface uplift due to tectonic processes within the basin and along the basin-bounding ranges. Despite the obvious inherent complexities involved when interpreting isotopes in precipitation records in regions, where fundamental changes in rainout regime have occurred over time, we are able to document parts of the uplift history of the intermontane Angastaco Basin and the impact of atmospheric flow conditions on stable isotope compositions in rainfall in this region. These relationships highlight the importance of evaluating possible causes for isotopic change in precipitation prior to modeling paleoelevations based on assumptions that may not apply to this type of environment. Importantly, similar conditions may be encountered in other intermontane-basin settings and broken-forelands with pronounced topographic and rainfall gradients, such as the Qilian Shan and Tian Shan of Central Asia, the Alborz mountains of northern Iran or the northern and northeastern margins of the Anatolian Plateau.

Acknowledgements

This research was funded by Deutsche Forschungsgemeinschaft (DFG) grants STR373/21-1 and STR373/16-1 to M. Strecker and MU2845/4-1 to A. Mulch who further acknowledges support through the LOEWE funding program of the Hessen State Ministry of Higher Education, Research, and the Arts. We thank J. Fiebig and U. Treffert (Frankfurt) for laboratory support. We are also grateful for constructive reviews provided by E. Cassel and T. Jordan.

Appendix A. Supplementary material

Supplementary material related to this article can be found online at http://dx.doi.org/10.1016/j.epsl.2016.02.009.

References

Allmendinger, R.W., Jordan, T.E., Kay, S.M., Isacks, B.L., 1997. The evolution of the Altiplano–Puna plateau of the Central Andes. Annu. Rev. Earth Planet. Sci. 25, 139–174. http://dx.doi.org/10.1146/annurev.earth.25.1.139.

Baker, P.A., Fritz, S.C., Dick, C.W., Eckert, A.J., Horton, B.K., Manzoni, S., Ribas, C.C., Garzione, C.N., Battisti, D.S., 2014. The emerging field of geogenomics: constraining geological problems with genetic data. Earth-Sci. Rev. 135, 38–47. http://dx.doi.org/10.1016/j.earscirev.2014.04.001.

Bona, P., Starck, D., Galli, C., Gasparini, Z., Reguero, M., 2013. Caiman cf. Latirostris (Alligatoridae, Caimaninae) in the late Miocene Palo Pintado Formation, Salta province, Argentina: paleogeographic and paleoenvironmental considerations. Ameghiniana 51, 25–36. http://dx.doi.org/10.5710/AMGH.11.12.2013.1507.

Bookhagen, B., Strecker, M.R., 2008. Orographic barriers, high-resolution TRMM rainfall, and relief variations along the eastern Andes. Geophys. Res. Lett. 35. http://dx.doi.org/10.1029/2007GL032011.

Bookhagen, B., Strecker, M.R., 2012. Spatiotemporal trends in erosion rates across a pronounced rainfall gradient: examples from the southern Central Andes. Earth Planet. Sci. Lett. 327–328, 97–110. http://dx.doi.org/10.1016/j.epsl.2012.02.005.

Bywater-Reyes, S., Carrapa, B., Clementz, M., Schoenbohm, L.M., 2010. Effect of late Cenozoic aridification on sedimentation in the Eastern Cordillera of northwest Argentina (Angastaco Basin). Geology 38, 235–238. http://dx.doi.org/10.1130/G30532.1.

Canavan, R.R., Carrapa, B., Clementz, M.T., Quade, J., Decelles, P.G., Schoenbohm, L.M., 2014. Early Cenozoic uplift of the Puna Plateau, Central Andes, based on stable isotope paleoaltimetry of hydrated volcanic glass. Geology 42, 447–450. http://dx.doi.org/10.1130/G35239.1.

Carrapa, B., Trimble, J.D., Stockli, D.F., 2011. Patterns and timing of exhumation and deformation in the Eastern Cordillera of NW Argentina revealed by (U–Th)/He thermochronology. Tectonics 30, TC3003. http://dx.doi.org/10.1029/2010TC002707.

Carrapa, B., Bywater-Reyes, S., Decelles, P.G., Mortimer, E., Gehrels, G.E., 2012. Late Eocene–Pliocene basin evolution in the Eastern Cordillera of northwestern Argentina (25°–26°S): regional implications for Andean orogenic wedge development. Basin Res. 24, 249–268. http://dx.doi.org/10.1111/j.1365-2117.2011.00519.x.

Carrapa, B., Huntington, K.W., Clementz, M., Quade, J., Bywater-Reyes, S., Schoenbohm, L.M., Canavan, R.R., 2014. Uplift of the Central Andes of NW Argentina associated with upper crustal shortening, revealed by multiproxy isotopic analyses. Tectonics 33, 1039–1054. http://dx.doi.org/10.1002/(ISSN)1944-9194.

Carrera, N., Muñoz, J.A., 2008. Thrusting evolution in the southern Cordillera Oriental (northern Argentine Andes): constraints from growth strata. Tectonophysics 459, 107–122. http://dx.doi.org/10.1016/j.tecto.2007.11.068.

Cassel, E.J., Graham, S.A., Chamberlain, C.P., 2009. Cenozoic tectonic and topographic evolution of the northern Sierra Nevada, California, through stable isotope paleoaltimetry in volcanic glass. Geology 37, 547–550. http://dx.doi.org/10.1130/G25572A.1.

Cassel, E.J., Breecker, D.O., Henry, C.D., Larson, T.E., Stockli, D.F., 2014. Profile of a paleo-orogen: high topography across the present-day Basin and Range from 40 to 23 Ma. Geology 42, 1007–1010. http://dx.doi.org/10.1130/G35924.1.

Chamberlain, C.P., Poage, M., Craw, D., Reynolds, R., 1999. Topographic development of the Southern Alps recorded by the isotopic composition of authigenic clay minerals, South Island, New Zealand. Chem. Geol. 155, 279–294. http://dx.doi.org/10.1016/S0009-2541(98)00165-X.

Coutand, I., Carrapa, B., Deeken, A., Schmitt, A.K., Sobel, E.R., Strecker, M.R., 2006. Propagation of orographic barriers along an active range front: insights from sandstone petrography and detrital apatite fission-track thermochronology in the intramontane Angastaco basin, NW Argentina. Basin Res. 18, 1–26. http://dx.doi.org/10.1111/j.1365-2117.2006.00283.x.

Deeken, A., Sobel, E.R., Coutand, I., Haschke, M., Riller, U., Strecker, M.R., 2006. Development of the southern Eastern Cordillera, NW Argentina, constrained by apatite fission track thermochronology: from early Cretaceous extension to middle Miocene shortening. Tectonics 25, TC6003. http://dx.doi.org/10.1029/2005TC001894.

del Papa, C.E., Hongn, F.D., Powell, J., Payrola-Bosio, P.A., Do Campo, M., Strecker, M.R., Petrinovic, I.A., Schmitt, A.K., Pereyra, R., 2013. Middle Eocene–Oligocene broken-foreland evolution in the Andean Calchaqui Valley, NW Argentina: insights from stratigraphic, structural and provenance studies. Basin Res. 25, 574–593. http://dx.doi.org/10.1111/bre.12018.

Dettinger, M.P., Quade, J., 2015. Testing the analytical protocols and calibration of volcanic glass for the reconstruction of hydrogen isotopes in paleoprecipitation. In: Geological Society of America Memoirs, vol. 212, pp. 261–276.

Fiorella, R.P., Poulsen, C.J., Pillco-Zolá, R.S., Barnes, J.B., Tabor, C.R., Ehlers, T.A., 2015. Spatiotemporal variability of modern precipitation δ^{18}O in the central Andes and implications for paleoclimate and paleoaltimetry estimates. J. Geophys. Res., Atmos. 120, 4630–4656. http://dx.doi.org/10.1002/2014JD022893.

Friedman, I., Gleason, J., Warden, A., 1993. Ancient climate from deuterium content of water in volcanic glass. In: Geophys. Monogr. Ser., vol. 78, pp. 309–319.

Galli, C.I., Anzótegui, L.M., Horn, M.Y., Morton, L.S., 2011. Paleoambiente y paleocomunidades de la Formación Palo Pintado (Mioceno–Plioceno), Provincia de Salta, Argentina. Rev. Mex. Cienc. Geol. 28, 161–174.

Galli, C.I., Coira, B., Alonso, R.N., Reynolds, J.H., Matteini, M., Hauser, N., 2014. Tectonic controls on the evolution of the Andean Cenozoic foreland basin: evidence from fluvial system variations in the Payogastilla Group, in the Calchaquí, Tonco and Amblayo Valleys, NW Argentina. J. South Am. Earth Sci. 52, 234–259. http://dx.doi.org/10.1016/j.jsames.2014.03.003.

Garreaud, R.D., Molina, A., Farías, M., 2010. Andean uplift, ocean cooling and Atacama hyperaridity: a climate modeling perspective. Earth Planet. Sci. Lett. 292, 39–50. http://dx.doi.org/10.1016/j.epsl.2010.01.017.

Garzione, C.N., Quade, J., Decelles, P.G., English, N.B., 2000. Predicting paleoelevation of Tibet and the Himalaya from δ^{18}O vs. altitude gradients in meteoric water across the Nepal Himalaya. Earth Planet. Sci. Lett. 183, 215–229. http://dx.doi.org/10.1016/S0012-821X(00)00252-1.

Gébelin, A., Mulch, A., Teyssier, C., Jessup, M.J., Law, R.D., Brunel, M., 2013. The Miocene elevation of Mount Everest. Geology 41, 799–802. http://dx.doi.org/10.1130/G34331.1.

Gregory-Wodzicki, K., 2000. Uplift history of the Central and Northern Andes: a review. Geol. Soc. Am. Bull. 112, 1091–1105. http://dx.doi.org/10.1130/0016-7606(2000)112<1091:UHOTCA>2.0.CO;2.

Hain, M.P., Strecker, M.R., Bookhagen, B., Alonso, R.N., Pingel, H., Schmitt, A.K., 2011. Neogene to Quaternary broken foreland formation and sedimentation dynamics in the Andes of NW Argentina (25°S). Tectonics 30. http://dx.doi.org/10.1029/2010TC002703.

Hoke, G.D., Garzione, C.N., 2008. Paleosurfaces, paleoelevation, and the mechanisms for the late Miocene topographic development of the Altiplano plateau. Earth Planet. Sci. Lett. 271, 192–201. http://dx.doi.org/10.1016/j.epsl.2008.04.008.

Hongn, F.D., del Papa, C.E., Powell, J., Petrinovic, I., Mon, R., Deraco, V., 2007. Middle Eocene deformation and sedimentation in the Puna–Eastern Cordillera transition (23°–26°S): control by preexisting heterogeneities on the pattern of initial Andean shortening. Geology 35, 271–274. http://dx.doi.org/10.1130/G23189A.1.

Hoorn, C., Guerrero, J., Sarmiento, G., Lorente, M., 1995. Andean tectonics as a cause for changing drainage patterns in Miocene northern South America. Geology 23, 237–240. http://dx.doi.org/10.1130/0091-7613(1995)023<0237:ATAACF>2.3.CO;2.

Hoorn, C., Wesselingh, F.P., Ter Steege, H., Bermudez, M.A., Mora, A., Sevink, J., Sanmartin, I., Sanchez-Meseguer, A., Anderson, C.L., Figueiredo, J.P., Jaramillo, C., Riff, D., Negri, F.R., Hooghiemstra, H., Lundberg, J., Stadler, T., Sarkinen, T., Antonelli, A., 2010. Amazonia through time: Andean uplift, climate change, landscape evolution, and biodiversity. Science 330, 927–931. http://dx.doi.org/10.1126/science.1194585.

Hren, M.T., Bookhagen, B., Blisniuk, P.M., Booth, A.L., Chamberlain, C.P., 2009. δ^{18}O and δD of streamwaters across the Himalaya and Tibetan Plateau: implications for moisture sources and paleoelevation reconstructions. Earth Planet. Sci. Lett. 288, 20–32. http://dx.doi.org/10.1016/j.epsl.2009.08.041.

Hynek, S.A., 2011. Mio–Pliocene geology of the southern Puna plateau margin, Argentina. PhD thesis. University of Utah.

Hynek, S.A., Passey, B.H., Prado, J.L., Brown, F.H., Cerling, T.E., Quade, J., 2012. Small mammal carbon isotope ecology across the Miocene–Pliocene boundary, northwestern Argentina. Earth Planet. Sci. Lett. 321–322, 177–188. http://dx.doi.org/10.1016/j.epsl.2011.12.038.

Isacks, B.L., 1988. Uplift of the Central Andean Plateau and bending of the Bolivian Orocline. J. Geophys. Res. 93, 3211–3231. http://dx.doi.org/10.1029/JB093iB04p03211.

Jordan, T.E., Alonso, R.N., 1987. Cenozoic stratigraphy and basin tectonics of the Andes Mountains, 20°–28° South Latitude. AAPG Bull. 71, 49–64. http://dx.doi.org/10.1306/94886D44-1704-11D7-8645000102C1865D.

Montero-López, C., Strecker, M.R., Schildgen, T.F., Hongn, F.D., Guzmán, S., Bookhagen, B., Sudo, M., 2014. Local high relief at the southern margin of the Andean plateau by 9 Ma: evidence from ignimbritic valley fills and river incision. Terra Nova 26, 454–460. http://dx.doi.org/10.1111/ter.12120.

Mulch, A., 2016. Stable isotope paleoaltimetry and the evolution of landscapes and life. Earth Planet. Sci. Lett. 433, 180–191. http://dx.doi.org/10.1016/j.epsl.2015.10.034.

Mulch, A., Teyssier, C., Cosca, M.A., Vanderhaeghe, O., Vennemann, T.W., 2004. Reconstructing paleoelevation in eroded orogens. Geology 32, 525. http://dx.doi.org/10.1130/G20394.1.

Mulch, A., Graham, S.A., Chamberlain, C.P., 2006. Hydrogen isotopes in Eocene river gravels and paleoelevation of the Sierra Nevada. Science 313, 87–89. http://dx.doi.org/10.1126/science.1125986.

Mulch, A., Sarna-Wojcicki, A.M., Perkins, M.E., Chamberlain, C.P., 2008. A Miocene to Pleistocene climate and elevation record of the Sierra Nevada (California). Proc. Natl. Acad. Sci. USA 105, 6819–6824. http://dx.doi.org/10.1073/pnas.0708811105.

Mulch, A., Uba, C.E., Strecker, M.R., Schoenberg, R., Chamberlain, C.P., 2010. Late Miocene climate variability and surface elevation in the central Andes. Earth Planet. Sci. Lett. 290, 173–182. http://dx.doi.org/10.1016/j.epsl.2009.12.019.

Pingel, H., Alonso, R.N., Mulch, A., Rohrmann, A., Sudo, M., Strecker, M.R., 2014. Pliocene orographic barrier uplift in the southern Central Andes. Geology 42, 691–694. http://dx.doi.org/10.1130/G35538.1.

Poage, M.A., Chamberlain, C.P., 2001. Empirical relationships between elevation and the stable isotope composition of precipitation and surface waters: considerations for studies of paleoelevation change. Am. J. Sci. 301, 1–15.

Polissar, P.J., Freeman, K.H., Rowley, D.B., McInerney, F.A., Currie, B.S., 2009. Paleoaltimetry of the Tibetan Plateau from D/H ratios of lipid biomarkers. Earth Planet. Sci. Lett. 287, 64–76. http://dx.doi.org/10.1016/j.epsl.2009.07.037.

Prohaska, F., 1976. The climate of Argentina, Paraguay and Uruguay. In: Schwerdtfeger, W. (Ed.), Climates in Central and South America. In: World Survey of Climatology, vol. 12. Elsevier, Amsterdam, pp. 13–73.

Quade, J., Garzione, C.N., Eiler, J.M., 2007. Paleoelevation reconstruction using pedogenic carbonates. In: Reviews in Mineralogy and Geochemistry, vol. 66, pp. 53–87. http://dx.doi.org/10.2138/rmg.2007.66.3.

Quade, J., Dettinger, M.P., Carrapa, B., DeCelles, P., Murray, K.E., Huntington, K.W., Cartwright, A., Canavan, R.R., Gehrels, G., Clementz, M., 2015. The growth of the central Andes, 22°S–26°S. In: DeCelles, P.G., Ducea, M.N., Carrapa, B., Kapp, P.A. (Eds.), Geodynamics of a Cordilleran Orogenic System: The Central Andes of Argentina and Northern Chile. In: Geological Society of America Memoirs, vol. 212, pp. 277–308. http://dx.doi.org/10.1130/2015.1212(14).

Reiners, P.W., Thomson, S.N., Vernon, A., Willett, S.D., Zattin, M., Einhorn, J., Gehrels, G., Quade, J., Pearson, D., Murray, K.E., Cavazza, W., 2015. Low-temperature thermochronologic trends across the central Andes, 21°S–28°S. In: DeCelles, P.G., Ducea, M.N., Carrapa, B., Kapp, P.A. (Eds.), Geodynamics of a Cordilleran Orogenic System: The Central Andes of Argentina and Northern Chile. In: Geological Society of America Memoirs, vol. 212, pp. 215–249. http://dx.doi.org/10.1130/2015.1212(12).

Rohrmann, A., Strecker, M.R., Bookhagen, B., Mulch, A., Sachse, D., Pingel, H., Alonso, R.N., Schildgen, T.F., Montero-López, C., 2014. Can stable isotopes ride out the storms? The role of convection for water isotopes in models, records, and paleoaltimetry studies in the central Andes. Earth Planet. Sci. Lett. 407, 187–195. http://dx.doi.org/10.1016/j.epsl.2014.09.021.

Romatschke, U., Houze, R.A., 2010. Extreme summer convection in South America. J. Climate 23, 3761–3791. http://dx.doi.org/10.1175/2010JCLI3465.1.

Romatschke, U., Houze, R.A., 2013. Characteristics of precipitating convective systems accounting for the summer rainfall of tropical and subtropical South America. J. Hydrometeorol. 14, 25–46. http://dx.doi.org/10.1175/JHM-D-12-060.1.

Rowley, D., Pierrehumbert, R., Currie, B.S., 2001. A new approach to stable isotope-based paleoaltimetry: implications for paleoaltimetry and paleohypsometry of the High Himalaya since the Late Miocene. Earth Planet. Sci. Lett. 188, 253–268.

Rowley, D.B., Garzione, C.N., 2007. Stable isotope-based paleoaltimetry. Annu. Rev. Earth Planet. Sci. 35, 463–508. http://dx.doi.org/10.1146/annurev.earth.35.031306.140155.

Saylor, J.E., Horton, B.K., 2014. Nonuniform surface uplift of the Andean plateau revealed by deuterium isotopes in Miocene volcanic glass from southern Peru. Earth Planet. Sci. Lett. 387, 120–131. http://dx.doi.org/10.1016/j.epsl.2013.11.015.

Schemmel, F., Mikes, T., Rojay, B., Mulch, A., 2013. The impact of topography on isotopes in precipitation across the Central Anatolian Plateau (Turkey). Am. J. Sci. 313, 61–80. http://dx.doi.org/10.2475/02.2013.01.

Starck, D., Anzótegui, L.M., 2001. The late Miocene climatic change – persistence of a climatic signal through the orogenic stratigraphic record in northwestern Argentina. J. South Am. Earth Sci. 14, 763–774. http://dx.doi.org/10.1016/S0895-9811(01)00066-9.

Strecker, M.R., Alonso, R.N., Bookhagen, B., Carrapa, B., Hilley, G.E., Sobel, E.R., Trauth, M.H., 2007. Tectonics and climate of the southern central Andes. Annu. Rev. Earth Planet. Sci. 35, 747–787. http://dx.doi.org/10.1146/annurev.earth.35.031306.140158.

Strecker, M.R., Alonso, R.N., Bookhagen, B., Carrapa, B., Coutand, I., Hain, M.P., Hilley, G.E., Mortimer, E., Schoenbohm, L.M., Sobel, E.R., 2009. Does the topographic distribution of the central Andean Puna Plateau result from climatic or geodynamic processes? Geology 37, 643–646. http://dx.doi.org/10.1130/G25545A.1.

Uba, C.E., Strecker, M.R., Schmitt, A.K., 2007. Increased sediment accumulation rates and climatic forcing in the central Andes during the late Miocene. Geology 35, 979–982. http://dx.doi.org/10.1130/G224025A.1.

Vera, C.S., Baez, J., Douglas, M., Emmanuel, C.B., Marengo, J., Meitin, J., Nicolini, M., Nogues-Paegle, J., Paegle, J., Penalba, O., 2006. The South American low-level jet experiment. Bull. Am. Meteorol. Soc. 87, 63–77. http://dx.doi.org/10.1175/BAMS-87-1-63.

Viramonte, J.G., Reynolds, J.H., del Papa, C.E., Disalvo, A., 1994. The Corte Blanco garnetiferous tuff: a distinctive late Miocene marker bed in northwestern Argentina applied to magnetic polarity stratigraphy in the Río Yacones, Salta Province. Earth Planet. Sci. Lett. 121, 519–531. http://dx.doi.org/10.1016/0012-821X(94)90088-4.

Zachos, J.C., Dickens, G.R., Zeebe, R.E., 2008. An early Cenozoic perspective on greenhouse warming and carbon-cycle dynamics. Nature 451, 279–283. http://dx.doi.org/10.1038/nature06588.